

Coherent trajectory through the normal-to-superconducting transition reveals ultrafast vortex dynamics in a superconductor.

P. Kusar¹, I. Madan¹, M. Lu-Dac¹, T. Mertelj¹, V. V. Kabanov¹, S. Sugai² and D. Mihailovic^{1,3}

¹*Complex Matter Department, Jozef Stefan Institute, Jamova 39, 1000 Ljubljana, Slovenia*

²*Department of Physics, Faculty of Science, Nagoya University,
Furo-cho, Chikusa-ku, Nagoya 464-8602, Japan and*

³*CENN Nanocentre, Jamova 39, 1000 Ljubljana, Slovenia*

(Dated: August 13, 2012)

We report on measurements of the trajectory of the superconducting order parameter $\psi(t)$ through the normal-to-superconductor transition in $\text{La}_{1.9}\text{Sr}_{0.1}\text{CuO}_4$ under ultrafast quench conditions up to 4×10^{14} K/s. Using a 3-pulse technique, we isolate the trajectory of $\psi(t)$ from single-particle processes on short timescales. Detailed modeling of the system trajectory using hot electron energy relaxation, time-dependent Ginzburg-Landau theory and vortex creation according to the Kibble-Zurek mechanism describes the experimental data in quantitative detail, significantly advancing our understanding of the behaviour of the normal-to-superconductor transition under highly nonequilibrium conditions. The recovery of ψ takes place on a timescale of 20 to 60 ps, depending on the excitation energy density, while the vortex dynamics is apparent on a timescale of $10 \sim 30$ ps and is visible only for the fastest quench rates.

What happens when a system goes through a symmetry-breaking transition depends crucially on how fast the transition occurs[1, 2]. If the quench process is sufficiently fast large numbers of topological defects are created and the nature of the final state can be substantially different than if the transition takes place slowly. The study of the time evolution of complex systems through symmetry breaking transitions (SBT) is thus of great fundamental interest in different areas of physics[2–4] and beyond. The diversity of microscopic vacua in condensed matter systems makes them excellent candidates for the experimental study of new phenomena[5], also posing new challenges for the general theory of SBTs. Of particular general interest is the normal-to-superconducting (N→S) state transition in which a Lorentz non-invariant system breaks gauge invariance[6]. Under near-equilibrium conditions the N→S transition occurs when the thermal fluctuation timescale τ_F becomes comparable to the “Ginzburg-Landau time” which for typical high temperature superconductors is $\tau_{GL} = \pi/\hbar(T - T_c) \simeq 10^{-12} - 10^{-13}$ s[2, 5, 7, 8]. The intrinsic collective system relaxation time τ_{GL} defines the relevant timescale and experimental resolution necessary to investigate system trajectories through the transition. Till now, the shortest quench times through the transition were $\tau_q \sim 10^{-8}$ s[9], which were relatively long compared to τ_{GL} , so observations were focused on statistical counts of vortices in the aftermath of the transition as a function of the quench rate $\gamma_q = 1/\tau_q$. Femtosecond laser spectroscopy offers sufficient time resolution for ultrafast quench studies and pump-probe transient reflectivity experiments have recently elucidated the *destruction* of superconductivity (i.e. the S→N transition)[10–12]. However, standard pump-probe techniques cannot distinguish the trajectory of the order parameter (OP) $\psi(t)$ from photo-excited hot carrier relaxation, quasiparticle

(QP) recombination dynamics across the superconducting gap and the relaxation of pseudogap (PG) excitations, all of which appear simultaneously in the time-resolved response[13–18].

To solve this problem we devised a 3 pulse technique shown schematically in Fig. 1 which allows us to measure in real time the superconducting order parameter $\psi(t)$ through the transition in a $\text{La}_{1.9}\text{Sr}_{0.1}\text{CuO}_4$ (LSCO) single crystal with ultrahigh quench rates of up to $\gamma_q = 1/\tau_q = (dT/dt) T_c^{-1} \simeq 4 \times 10^{14} \text{ s}^{-1}$. Furthermore, we can vary γ_q by changing the laser excitation energy. We compare the data with predictions of the Kibble-Zurek (K-Z) mechanism of vortex creation, finding evidence for ultrafast vortex dynamics in the rapid quench regime when $\tau_q \sim \tau_{GL}$ [1, 20]. $\text{La}_{1.9}\text{Sr}_{0.1}\text{CuO}_4$ is chosen because it is one of the best studied superconductors particularly by femto-optical methods.[10, 14, 27]

With our technique the superconducting state is first rapidly nonthermally[10] destroyed in ~ 1 ps by an intense “destruction” (D) laser pulse creating a pancake-like normal region defined by the laser beam profile with the FWHM diameter $d = 60 \mu\text{m}$ and the optical penetration length $\lambda_p = 150 \text{ nm}$ (at 800nm). We then monitor the recovery of the OP by means of the transient reflectivity $\Delta R(\Delta t_{2-3})/R$ excited with a weaker pump (P) pulse and probed with even weaker probe (p) pulse as a function of time delay Δt_{1-2} between the D and P pulse (see Fig. 1).[19] The D pulse fluence is adjusted to achieve different quench rates.

After destruction, an OP front propagates from the bulk towards the surface on a timescale $\tau_\psi \sim \lambda_p/v_\psi \sim \lambda_p\tau_{GL}/\xi_\perp \sim 10^3\tau_{GL}$, where v_ψ is the OP front velocity[32] and ξ_\perp is the out-of-plane SC correlation length. τ_ψ is much longer than both, the quench time τ_q and the Zurek time $\tau_Z \sim \sqrt{\tau_q\tau_{GL}}$. As a consequence the normal region is supercooled and we can expect vor-

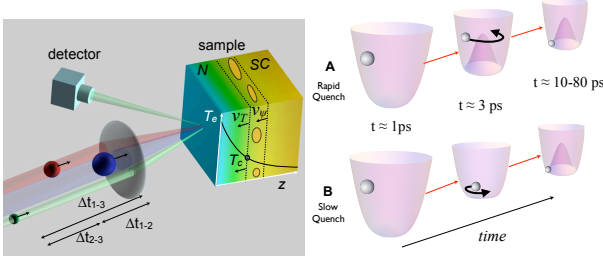


Figure 1: a) A schematic diagram of the pulse sequence. The time delays Δt_{1-2} , Δt_{1-3} and Δt_{2-3} refer to delays between the D pulse (blue) and the P pulse (red), the D pulse and the probe pulse (green) and between the P pulse and the probe pulse, respectively. The temperature front where $T_e = T_c$ and the S/N phase boundary move with velocities v_T and v_ψ respectively. Vortices are created in the wake of the temperature front. b) The system trajectory (depicted by the silver ball) in a temporally evolving potential. In the rapid quench scenario (A), the potential changes faster than the system can follow. The opposite is true in the slow quench scenario (B).

tex formation according to the K-Z scenario.[1, 5, 9, 20–22] Depending on the quench conditions, the propagating velocity of the temperature $T = T_c$ front v_T can be either faster or slower than the critical velocity[20] $v_{\text{crit}} \approx v_\psi \sqrt{\tau_{\text{GL}}/\tau_q} \lesssim 10^5$ cm/s. In the ultrafast quench limit when $v_T > v_{\text{crit}}$, we expect vortex formation, while in the slow quench limit ($v_T < v_{\text{crit}}$), vortex formation becomes suppressed [20, 22].

The time-evolution of the electronic and lattice temperatures $T_e(t)$ and $T_L(t)$ respectively, which govern the quench process, are calculated using the standard two-temperature model[23, 26]: $\gamma_e T_e \frac{dT_e}{dt} = -\gamma_L (T_e - T_L) + E(t)$ and $C_L(T) \frac{dT_L}{dt} = \gamma_L (T_e - T_L)$, where $E(t)$ is a function (Gaussian) describing the energy density per unit time supplied by the laser pulse [33]. For maximum accuracy we used the temperature-dependent thermal constants $\gamma_e(T)$ and $C_L(T)$ from experimental data[25] and the measured energy loss rate $\gamma_L \simeq 340$ K/ps for $\text{La}_{1.9}\text{Sr}_{0.1}\text{CuO}_4$ [24]. The dependence of $T_e(t)$ and $T_L(t)$ on the D pulse fluence, \mathcal{F}_D , is shown in Fig. 2a) for the first 2.5 picoseconds. The red contour lines show when either T_e or T_L crosses T_c , which is the critical point of the quench.

For low $\mathcal{F}_D \leq 15 \mu\text{J}/\text{cm}^2$, we have a rapid quench scenario as T_e rapidly crosses T_c within a few hundred femtoseconds, the quench rate being governed by the electronic energy relaxation rate $\gamma_q \simeq \gamma_e \simeq 4 \times 10^{14}$ K/s. For $\mathcal{F}_D > 15 \mu\text{J}/\text{cm}^2$ however, the lattice is heated above T_c by the D pulse, so the cooling rate through T_c is governed by diffusion processes on timescales longer than ~ 30 ps. Thus by changing \mathcal{F}_D we can effectively vary the regime from rapid to slow quench, over a very wide range of quench times from $\tau_q = 100$ fs to hundreds of picoseconds.

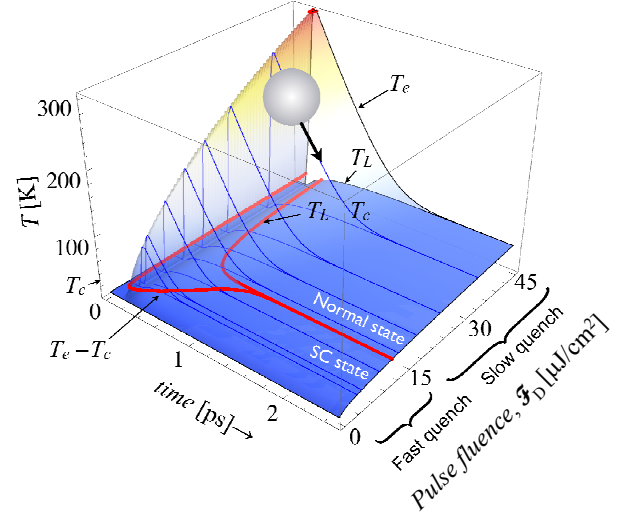


Figure 2: The time evolution of the electronic and lattice temperatures T_e and T_L respectively. The ball signifies the trajectory of $T_e(t)$ for a D pulse fluence $\mathcal{F}_D = 38 \mu\text{J}/\text{cm}^2$. The blue lines are the trajectories of $T_e(t)$ corresponding to the D pulse fluences used in the experiments. The red lines signify the time when T_e and T_L cross the critical temperature $T_c = 30$ K. Rapid quench occurs for $\mathcal{F}_D < 15 \mu\text{J}/\text{cm}^2$.

The transient reflectivity amplitude in the superconducting state is proportional to the square of the order parameter $A_s = \Delta R/R \propto |\psi(t_{1-2})|^2$ [19], so to detect the trajectory $\psi(t)$ through T_c , we measure the transient reflectivity by the Pump-probe technique at different time delays after the D pulse. The experimental data on the transient reflectivity $\Delta R(\Delta t_{2-3})/R$ at different delays Δt_{1-2} during the system recovery is shown in Fig. 3a). Two distinct and easily identifiable contributions are observed: one has a peak around 0.2 ps which has been previously identified to be due to pseudogap excitations, and the other is the QP recombination signal of the superconducting condensate with a peak near 2 ps, extending to tens of ps[14, 27]. We observe a clear suppression of the QP peak at short delay Δt_{1-2} and a gradual emergence of the SC state with increasing delay. A distinct feature in Fig. 3a) is the convergence of all QP curves after a delay $\Delta t_{2-3} = \tau_{\text{th}} \simeq 25$ ps which corresponds to the complete thermalization of all degrees of freedom.

For further analysis, we subtract the PG response from the data[34] and plot A_s as a function Δt_{1-2} , thus obtaining the trajectory of $|\psi(t)|^2$ shown by the square black dots in Fig. 3b). From the exponential fits of the decay of $\Delta R/R(t_{2-3})$ we also obtain the QP relaxation time τ_{QP} as a function of Δt_{1-2} which is shown in Fig 3b), plotted as a relaxation rate $1/\tau_{\text{QP}}$. We observe that $1/\tau_{\text{QP}}$ shows a similar trajectory as the order parameter; indeed superimposing $|\psi(t_{1-2})|$ on the graph of $1/\tau_{\text{QP}}(t_{1-2})$ (solid line in Fig. 3b)), we see that the QP recombination

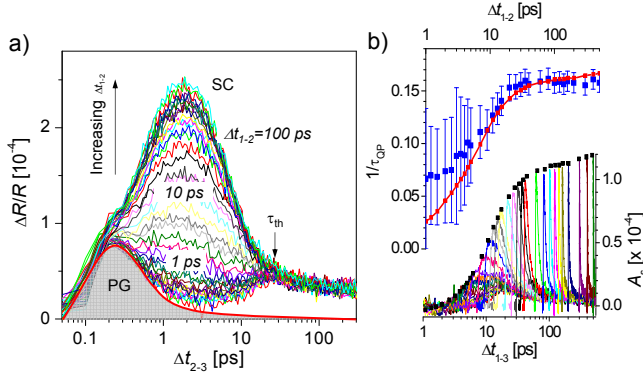


Figure 3: The transient reflectivity data $\Delta R/R$ for $\text{La}_{1.9}\text{Sr}_{0.1}\text{CuO}_4$ at 4 K as a function of Δt_{2-3} , for different Δt_{1-2} . The D pulse fluence is $\mathcal{F}_D = 12 \mu\text{J}/\text{cm}^2$, which is approximately three times above the destruction threshold ($\mathcal{F}_D \simeq 4 \mu\text{J}/\text{cm}^2$) [10]. The red line indicates the pseudogap signal measured above T_c . The recovery time of the SC state τ_{rec} is indicated. b) The same data as in a) after subtraction of the PG signal plotted as a function of Δt_{1-3} . The black squares are the fitted maximum amplitudes of A_s and give $|\psi(t)|^2$ for each Δt_{1-2} . The blue squares are the QP relaxation rate superimposed on the measured order parameter trajectory $|\psi(t)| \propto \sqrt{A_s}$ as a function of delay Δt_{1-2} .

rate closely follows the order parameter as a function of Δt_{1-2} , consistent with the fact that $1/\tau_{\text{QP}}(t)$ is proportional to the superconducting gap $\Delta_s(t)$, which is in turn proportional to $|\psi(t)|$ [13].

Tuning \mathcal{F}_D significantly changes the trajectory of the system through the transition, and the SC state recovers much more slowly with increasing \mathcal{F}_D . Fig. 4a) shows the trajectory of $|\psi|^2$ for a number of different \mathcal{F}_D . [35] For the lowest two values of \mathcal{F}_D , which correspond to the fastest quench, we see that destruction of the condensate is incomplete throughout the entire excitation volume, since $|\psi|^2$ is non-zero in the first 2 ps after the D pulse. With increasing \mathcal{F}_D the recovery becomes slower. The initial recovery rate $1/\tau_i$ can be obtained from the initial slope of $|\psi(\Delta t_{1-2})|^2$ for small Δt_{1-2} and is shown in Fig. 4b). Plotting the recovery time versus \mathcal{F}_D in Fig 4c), we find a phenomenological τ_i which increases approximately linearly with \mathcal{F}_D before eventually saturating at high \mathcal{F}_D . For comparison, we see that the QP recombination time τ_{QP} (shown on the same plot) first dramatically decreases below the destruction threshold fluence for $\mathcal{F}_D < 4 \mu\text{J}/\text{cm}^2$, and then slightly increases with increasing \mathcal{F}_D . This impressively demonstrates how well we can separate the order parameter recovery from τ_{QP} in these experiments, and more importantly, shows that the QP relaxation has very different systematics and plays no significant role in determining the recovery dynamics.

To analyze the trajectory of the system through the transition as accurately as possible, we use the full set

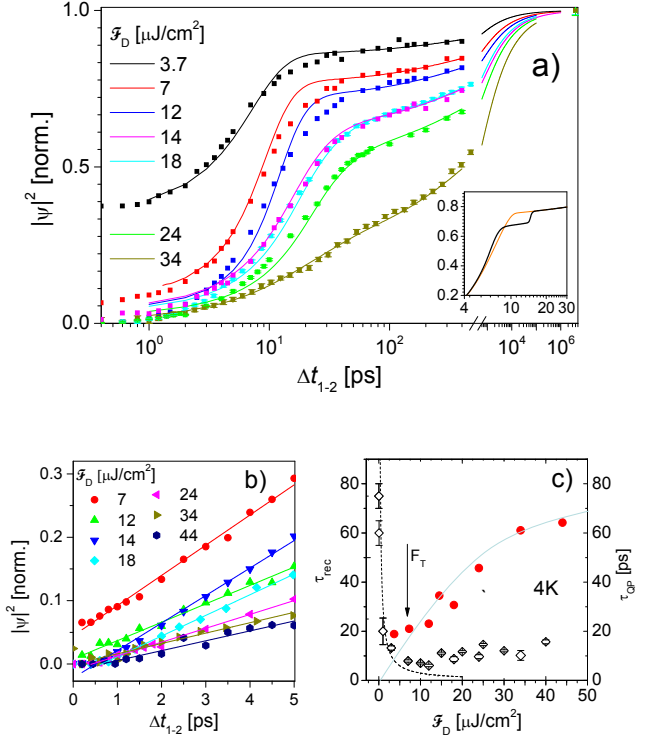


Figure 4: a) The trajectories of $|\psi|^2$ as a function of Δt_{1-2} for different D pulse fluences \mathcal{F}_D . The lines are calculated trajectories from the TDGL theory. The insert shows the predicted $|\psi(t)|^2$ with (black) and without (orange) vortices at $7 \mu\text{J}/\text{cm}^2$. The vertical scales are normalized to the equilibrium $|\psi_0|^2$ in the absence of the D pulse. b) The relaxation of $|\psi|^2$ in the first 5 ps for different fluences. c) The dependence of the recovery time τ_{rec} on pulse fluence (red dots). For comparison, the QP recombination time τ_{QP} is also shown for different \mathcal{F}_D (diamonds). The dashed line is the predicted τ_{QP} from the Rothwarf-Taylor model [28, 29] which is valid only below the destruction threshold $\mathcal{F}_D < 4 \mu\text{J}/\text{cm}^2$.

of TDGL equations where in the absence of an external field, the dimensionless order parameter $\psi(t)$ is described by [30]:

$$u \left(\frac{\partial \psi}{\partial t} + i\Phi\psi \right) = -\alpha_r(t, z)\psi - \psi|\psi|^2 + \nabla^2\psi + \eta, \quad (1)$$

$$\nabla^2\Phi = -\nabla \left[\frac{i}{2} (\psi^* \nabla\psi - \psi \nabla\psi^*) \right], \quad (2)$$

where temporal and spatial coordinates are measured in units of τ_{GL} and correlation length ξ , respectively. The only parameter in the equation is the ratio $u = \frac{\tau_{\text{GL}}}{\tau_\theta}$ between the longitudinal relaxation time and the transverse relaxation time. For our LSCO sample, $\tau_\theta \approx 1$ ps, $u \approx 5$ [8] and $\xi \approx 2$ nm. To initiate vortex formation arising from microscopic fluctuations, the customary Langevin noise term η is added [31]. We also take into account the inhomogeneous nature of light penetration into the sample and thermal diffusion processes, which take place on

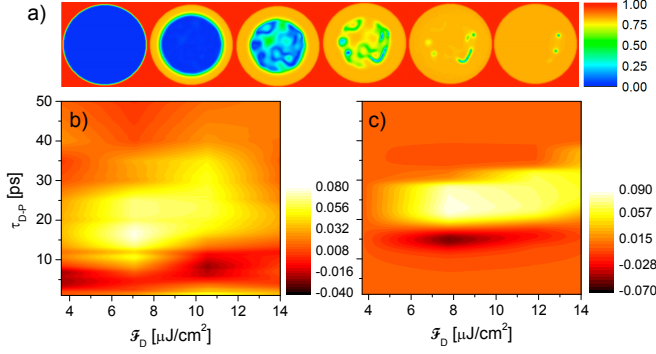


Figure 5: a) The predicted vortex structure of $|\psi|^2$ at different delay times corresponding to rapid quench conditions ($\mathcal{F}_D = 12 \mu\text{J}/\text{cm}^2$) showing the $|\psi(r, t)|^2$ in the time interval $\Delta t_{1-2} = 0 - 25$ ps in an area of $200 \times 200 \xi^2$. b) The difference between the experimental trajectory and the fits calculated without Langevin noise: $\Delta|\psi|^2 = |\psi|_{\text{novortex}}^2 - |\psi|_{\text{exp}}^2$ shows a clear suppression of $|\psi|^2$ around 10-20 ps for $5 < \mathcal{F}_D < 12 \text{ J}/\text{cm}^2$. c) the predicted suppression of $\Delta|\psi|_{\text{theory}}^2 = |\psi|_{\text{novortex}}^2 - |\psi|_{\text{vortex}}^2$ due to vortex formation around 10-20 ps introduced by fluctuations.

timescales beyond 10-30 ps by including a solution to the heat diffusion equation $\frac{\partial T_{\text{diff}}(t, \mathbf{s})}{\partial t} = D(T) \nabla^2 T_{\text{diff}}$, where $D(T) = k/\rho C_L$ is the diffusion coefficient, ρ is the density, k is the thermal conductivity. Solving for diffusion into the sample, we obtain a quench function applicable for long times. A simplified quench function can now be introduced in the TDGL equations:

$$\alpha_r(t, z) = -1 + \eta_L \frac{e^{\left(\frac{-z^2}{4Dt + \lambda_p^2}\right)} \lambda_p}{\sqrt{4Dt + \lambda_p^2}} + \eta_e e^{-z^2/\lambda_e^2} e^{-t/\tau_i}, \quad (3)$$

where the second term is a simplified solution to the diffusion equation in the limit of negligible lateral diffusion, and the last term approximates the trajectory of $T_e(t)$ shown in Fig. 2a). The fitting parameters are the two constants η_L and η_e . In Fig. 4a) we first compare the fits of the calculated trajectories with the data using Eq. 2 with $\eta = 0$. The fits are seen to be impressively good over the entire trajectory for high values of \mathcal{F}_D , but fail in a region around 10-20 ps for low \mathcal{F}_D . (Note that this discrepancy is extremely reproducible and well above the noise level). It is not possible to remove this discrepancy by changing *any* of the parameters of the model fit. Considering the low scatter of the data and the quality of the fits for higher \mathcal{F}_D it is clear that the persistent suppression of $|\psi|^2$ around 10-20 ps in the fast quench regime is a real effect.

Next, we include η in the calculation, initiating vortex formation. The resulting vortex structure is shown in Fig. 5a) in a sequence of snapshots using the parameters for the trajectory at $\mathcal{F}_D = 12 \mu\text{J}/\text{cm}^2$. The suppression of

$|\psi|^2$ by vortices calculated for different \mathcal{F}_D is compared with the experimentally observed effect in Fig. 5 b) and c) showing a remarkable agreement with the data around 10-20 ps and $\mathcal{F}_D < 14 \mu\text{J}/\text{cm}^2$. Intrinsic vortex-antivortex creation and annihilation dynamics is predicted precisely in the region in time and pulse fluence \mathcal{F}_D (i.e. quench rate) where the data show deviations from the homogeneous trajectory. In contrast to previous studies[9, 21], the experimental vortex density (Fig. 5b) appears to be in reasonable quantitative agreement with the calculated K-Z vortex density (Fig. 5c).

To conclude, we have found that macroscopic phenomenological modeling can accurately describe the data very well without resort to microscopic theory provided we include vortex dynamics within the Kibble-Zurek scenario. The microscopic phenomenology may be thought to be included in the quench function, which includes the effect of the quasiparticle relaxation bottleneck appearing as a result of the formation of a gap in the superconducting state. One may try and introduce modifications to the quench function, but these would have no transparent physical meaning within the present context. An alternative microscopic description would require a complete microscopic theory. The fact that no external adjustable parameters - other than those of the noise - are needed to achieve this agreement is attributed to the great care taken to accurately model the quench process and inhomogeneity. The vortex-antivortex pair generation rate according to the Kibble-Zurek scenario[20, 22] is proportional to $\tau_q^{-\sigma}$, where $\sigma = 0.25 \sim 0.5$ [20], consistent with the model fits and the observed suppression of ψ under ultrafast quench conditions. We have demonstrated that our new experimental technique opens the way to real-time studies of the order parameter trajectory and vortex dynamics in superconductors, giving information which is not available from other time resolved methods, and shows that modeling by use of TDGL equations can give a faithful description of the basic phenomena presented here for the first time. We end by noting that the significance of the dependence of τ_i on \mathcal{F}_D needs to be clarified, which can only be done by further systematic studies of other systems.

We wish to acknowledge the useful discussion with T.W. Kibble regarding the importance of a variable quench rate experiment.

-
- [1] T.W.B. Kibble, *J Phys A-Math Gen* **9**, 1387-1398 (1976).
 - [2] G. Volovik. *The Universe in a Helium Droplet*, Oxford University Press, 526 (2002).
 - [3] P.W. Higgs, *Physical Review* **145**, 1156-1163 (1966).
 - [4] Yu. M. Bunkov, and H. Godfrin, Eds. *Topological defects and the Non-Equilibrium Dynamics of Symmetry-Breaking Phase Transitions*, NATO ASI Series, ed. Kluwer Academic Publishers, (2000).

- [5] W. Zurek, *Nature* **317**, 505 (1985).
- [6] C.M. Varma, *J. Low Temp. Phys.* **126**, 901-909 (2002).
- [7] A.Schmid and G. Schön, *J Low Temp Phys* **20**, 207–227 (1975).
- [8] Albert Schmid, *Zeitschrift für Physik B Condensed Matter (Phys. Kondens. Mater.)*, **5**, 302 (1966), L. Kramer and R. J. Watts-Tobin, *Phys. Rev. Lett.* **40**, 1041 (1978).
- [9] D. Golubchik, E. Polturak, & G. Koren, *Phys. Rev. Lett.* **104**, 247002 (2010).
- [10] P. Kusar, V.V. Kabanov, J. Demsar, T. Mertelj and D.Mihailovic, *Phys. Rev. Lett.* **101**, 227001 (2008).
- [11] C. Giannetti et al., *Phys. Rev. B* **79**, 224502 (2009).
- [12] L. Stojchevska et al., *Phys. Rev. B* **84**, 180507(R) (2011).
- [13] V. Kabanov, J. Demsar, B. Podobnik & D. Mihailovic, *Phys. Rev. B* **59**, 1497–1506 (1999).
- [14] P. Kusar, J. Demsar, D. Mihailovic, & S. Sugai, *Phys. Rev. B* **72**, 014544 (2005).
- [15] G. P. Segre, et. al., *Phys. Rev. Lett.* **88**, 137001 (2002).
- [16] L. Perfetti et al., *Phys. Rev. Lett.* **99**, 197001 (2007), R. Cortes et al., *Phys. Rev. Lett.* **107**, 097002 (2011).
- [17] Y. H. Liu, Y. Toda, K. Shimatake, N. Momono, M. Oda, M. Ido, *Phys. Rev. Lett.* **101**, 137003 (2008).
- [18] C. Giannetti, et al., *Nat. Comm.* **2**, 353 (2011).
- [19] R. Yusupov, et al., *Nat. Phys.* **6**, 681–684 (2010).
- [20] T.W.B.Kibble and G.E.Volovik, *JETP Lett.*, **65**, 103 (1997).
- [21] R. Monaco, J. Mygind, M. Aaroe, R.J. Rivers, & V.P. Koshelets, *Phys. Rev. Lett.* **96**, 180604 (2006).
- [22] I. Aranson, N. Kopnin, & V. Vinokur, *Phys. Rev. Lett.* **83**, 2600–2603 (1999).
- [23] P.B. Allen, *Phys. Rev. Lett.* **59**, 1460 (1987).
- [24] C. Gadermaier, et al, *Phys. Rev. Lett.* **105**, 257001 (2010).
- [25] Hai-Hu Wen et al., *Phys. Rev.* **B70**, 214505, (2004).
- [26] V.V. Kabanov & A.S.Alexandrov, *Phys Rev* **B78**, 174514 (2008).
- [27] P. Kusar et al., *J Supercond Nov Magn* **24**, 421–425 (2010).
- [28] A. Rothwarf & B. Taylor, *Phys. Rev. Lett.* **19**, 27 (1967).
- [29] V. Kabanov, J. Demsar & D. Mihailovic, *Phys. Rev. Lett.* **95**, 147002 (2005).
- [30] L. P. Gor'kov and N. B. Kopnin. *Soviet Physics Uspekhi*, **18**, 496 (1975).
- [31] M.LuDac and V.V. Kabanov, *Phys. Rev.* **B79**, 184521 (2009).
- [32] The 1-D time dependent GL equation $\tau_{GL}\dot{\psi} = \xi^2\psi'' + (1 - T/T_c)\psi - \psi^3$ has a propagating soliton solution $\psi \propto \tanh[(v_\psi t - z)/w] - 1$ where $w = 2\sqrt{2}\xi/\sqrt{1 - T/T_c}$ and $v_\psi = 3\xi\sqrt{1 - T/T_c}/\sqrt{2}\tau_{GL}$. Taking $\xi \sim \xi_\perp \sim 0.2$ nm and $\tau_{GL} \sim 100$ fs gives $v_\psi \sim 10^5$ cm/s.
- [33] Although the electron energy relaxation model is known to fail at very early times because of Pauli blocking of the e - e scattering rate[24, 26], by the time of the quench - i.e. when T_e crosses T_c - it is expected to faithfully reproduce the cooling process.
- [34] The PG response in LSCO shows a clear T-dependence, which we have characterised as a function of T, doping and \mathcal{F} in references [14, 27]. Although the subtraction gives some uncertainty of the amplitude on timescales up to 1 ps, this is not relevant for the trajectory of ψ and the SC state recovery, which takes place beyond 1 ps.
- [35] We normalize A_S by its value in the absence of the D pulse to obtain dimensionless $|\psi(t_{1-2})|^2$.